






# A Study of Dimmings, CMEs, and Flares during the STEREO-SOHO Quadrature

Larisa D. Krista<sup>1,2,3</sup> , Drew Manning<sup>4</sup> , and Matthew J. West<sup>5</sup> <sup>1</sup>Cooperative Institute for Research in Environmental Sciences, University of Colorado, Boulder, CO 80309, USA; [larisa.krista@colorado.edu](mailto:larisa.krista@colorado.edu)<sup>2</sup>National Centers for Environmental Information, National Oceanic and Atmospheric Administration, Boulder, CO 80305, USA<sup>3</sup>Space Science Institute, Boulder, CO 80301, USA<sup>4</sup>Colorado College, Colorado Springs, CO 80903, USA<sup>5</sup>Southwest Research Institute, 1050 Walnut Street, Suite 300, Boulder, CO 80302, USA

Received 2022 March 16; revised 2022 April 13; accepted 2022 April 16; published 2022 May 17

## Abstract

During the *quadrature period* (2010 December–2011 August) the STEREO-A and B satellites were approximately at right angles to the SOHO satellite. This alignment was particularly advantageous for determining the coronal mass ejection (CME) properties, since the closer a CME propagates to the plane of sky, the smaller the measurement inaccuracies are. Our primary goal was to study dimmings and their relationship to CMEs and flares during this time. We identified 53 coronal dimmings using STEREO/EUVI 195 Å observations, and linked 42 of the dimmings to CMEs (observed with SOHO/LASCO/C2) and 23 to flares. Each dimming in the catalog was processed with the Coronal Dimming Tracker which detects transient dark regions in extreme ultraviolet images directly, without the use of difference images. This approach allowed us to observe *footpoint dimmings*: the regions of mass depletion at the footpoints of erupting magnetic flux rope structures. Our results show that the CME mass has a linear, moderate correlation with dimming total EUV intensity change, and a monotonic, moderate correlation with dimming area. These results suggest that the more the dimming intensity drops and the larger the erupting region is, the more plasma is evacuated. We also found a strong correlation between the flare duration and the total change in EUV intensity. The correlation between dimming properties showed that larger dimmings tend to be brighter; they go through more intensity loss and generally live longer—supporting the hypothesis that larger transient open regions release more plasma and take longer to close down and refill with plasma.

*Unified Astronomy Thesaurus concepts:* [Solar flares \(1496\)](#); [Solar coronal mass ejections \(310\)](#); [Solar ultraviolet emission \(1533\)](#)

## 1. Introduction

Coronal dimmings are commonly observed in extreme ultraviolet (EUV) wavelengths and are considered the footpoints of an erupting magnetic flux rope structure. During the eruption the plasma evacuates the low corona, and the decreased density leads to reduced emission in EUV and X-ray wavelengths. Hence, dimmings (i.e., transient coronal holes) appear as dark regions in EUV observations. The erupting plasma—also known as the coronal mass ejection or CME—is often observed in white-light coronagraph images. Dimmings have the potential to advance our understanding of the initiation, evolution, and resulting properties of CMEs. Our goal is to investigate the characteristic parameters of coronal dimmings and also identify any relationships with their corresponding eruptive counterparts (CMEs and flares). Dimming regions could also help us forecast the properties of CMEs propagating into interplanetary space. This is particularly important in the case of Earth-directed CMEs when coronagraph observations are not available from multiple viewpoints.

Several research teams have investigated the relationship between dimmings and their eruptive counterparts in the recent years. Utilizing data from the quadrature period, López et al. (2019) compared the CME masses calculated from white-light STEREO/COR2 images with estimated mass evacuated from

the associated dimming regions. They used the differential emission measure (DEM) technique to measure the mass loss from the EUV low corona using 32 dimmings identified in SDO/AIA images. The median of the relative error in absolute value between the masses predicted by their method and those calculated from white-light data is around 30%. In 75% of the events the absolute relative error was under 51%. This high level of uncertainty is likely due to a number of factors: the amount of material that gets piled up as the CME propagates away from the Sun, any additional mass evacuated from the dimming region during the eruption, and limitations in the mass-loss estimation from the EUV data.

Using a thresholding technique on logarithmic base-ratio images, Dissauer et al. (2018a) investigated the properties of two dimmings and found a relationship with the associated flares and CMEs. They separated the core and secondary dimmings based on the time of their appearance and a set threshold. They associated the core dimming with the footpoints of the erupting flux rope, while they related the secondary dimming with the CME expansion, formed by the evacuating plasma. They found that the start of the impulsive growth rate of the dimming was co-temporal with the flare onset and the rise of the CME. They also state that the difference in the dimming area and the magnetic flux magnitude was indicative of different CME masses.

In another 2018 study Dissauer et al. (2018b) analyzed the properties of 62 dimming events identified during the quadrature period in SDO/AIA observations and compared them with basic flare quantities. Using difference images, they defined *core dimmings* during the early phase of the dimming



Original content from this work may be used under the terms of the [Creative Commons Attribution 4.0 licence](#). Any further distribution of this work must maintain attribution to the author(s) and the title of the work, journal citation and DOI.

expansion as the darkest pixels in terms of absolute and relative intensity change in minimum intensity maps. For 60% of the events they identified such core dimmings, which they regarded as the footpoints of the erupting flux rope. However, it is unclear why no core dimmings were found in the remaining 40% of the cases. Further investigation would be beneficial to compare these difference-image core dimmings with directly observed EUV footpoint dimmings. The core dimmings in their study contained approximately 20% of the total flux but only accounted for 5% of the total dimming area. They found that the dimming area, the total dimming brightness, and the total unsigned magnetic flux had a strong correlation with the flare soft X-ray fluence. Soft X-ray fluence is the product of the peak flux and the flare duration, and is a measure of the total flare radiation loss in the 1–8 Å band. The results suggest that larger X-ray fluence is linked to larger, darker dimmings and higher magnetic flux. In a separate paper, Dissauer et al. (2019) discusses the relationship between a subset of the above discussed dimmings and their associated CMEs. They found that the area, total unsigned magnetic flux, and the total brightness of the dimmings show a strong correlation with the CME masses (41 events). The dimming mean intensity, area growth rate, the total magnetic flux rate was also found to be strongly correlated with the CME peak velocity (37 events). Based on these results the authors hypothesize that CMEs that are initiated lower in the corona are likely to propagate faster.

While it is not straightforward to compare results obtained with different detection methods, it is now more widely accepted that dimmings consist of two parts known as the inner *footpoint dimming* (aka *core* or *primary* dimming) that corresponds to the mass evacuation site at the erupting loop structure footpoints; and the outer *projection dimming* (aka *secondary* dimming) that corresponds to the fainter intensity reduction caused by the rising CME plasma plume. In this paper we use the terminology *footpoint* and *projection* dimming since these terms are descriptive of the physical phenomena (Krista & Reinard 2017). These two dimming parts are harder to discern in difference images, as the intensity change happens continuously as the plasma evacuates the footpoint region and becomes the more diffuse, low density rising plasma. In direct EUV observations only the footpoint dimming is observable due to the large density and intensity drop in the evacuation site (this region is essentially a temporary open magnetic field region or transient coronal hole). The projection dimming is not detected in direct EUV observations because the rising CME plasma is low density and it propagates in front of the denser, brighter background, which consists predominantly of closed magnetic field structures.

Our previous study (Krista & Reinard 2017) was based on the direct observation of dimmings using SDO/AIA data. 154 footpoint dimmings were identified and tracked using the Coronal Dimming Tracker (CoDiT) algorithm. 64 of the dimmings were linked with CMEs and 41 with flares. The results of the study showed that larger dimming regions have longer lifetimes and they take longer to open up and close down. Also, smaller dimmings acquire a higher magnetic flux imbalance and become more unipolar during their growth phase. We found that the brighter the dimming was pre-eruption and/or the darker the dimming became, the larger the CME mass was. Also, the change in the EUV intensity showed a nonlinear, moderate positive correlation with the CME mass, width, and flare duration. In this study no correlation was found

between the dimming area and the CME mass. These findings support the idea that the more the intensity drops in a dimming region, the larger the eruptive event is likely to be. The CMEs were detected using SOHO/LASCO/C2 and their masses were obtained from the CDAW catalog ([https://cdaw.gsfc.nasa.gov/CME\\_list/](https://cdaw.gsfc.nasa.gov/CME_list/)). It is important to note that in the CDAW catalog the CME masses are calculated assuming that the CMEs travel along the plane of sky (POS), which is often not the case. And the larger the CME propagation angle is relative to the POS, the more the Thomson scattering drops, and the larger the uncertainties become in the mass determination (Vourlidis et al. 2010).

In the work presented here, we introduce a major improvement compared to our previous work: we study CMEs that propagate close to the POS, while previously we studied CMEs that occurred at any angle between 0° and 90° from the POS. We were able to introduce this improvement by analyzing data obtained from the quadrature period. The dimmings—phenomena intrinsically related to CMEs—were detected near the disk center in STEREO-A and -B observations, and the CMEs in the POS in SOHO/LASCO images. The quadrature alignment occurred from 2010 December–2011 August, when the angle between STEREO-A/B and SOHO was 85°–95°. This, and further technical aspects of our work are detailed in Section 2. Our findings are laid out in Section 3 and we conclude by discussing the results in Section 4.

## 2. Instruments, Observations, and Data Analysis

We used observations from the Extreme Ultraviolet Imager (EUVI; Wuelser et al. 2004) instrument onboard the Solar Terrestrial Relations Observatory spacecraft (STEREO; Driesman et al. 2008) to identify and track coronal dimmings. EUVI is a normal incidence Ritchey—Chrétien telescope with a 2048 × 2048 pixel detector and a pixel size of 1"59. It observes a field of view that extends to 1.7  $R_{\odot}$ . It has four spectral channels (Fe IX 171 Å, Fe XII 195 Å, Fe XV 284 Å, and He II 304 Å) that observe the 0.05–20 MK temperature range. We used the 195 Å wavelength, which shows a higher contrast between the cooler, low density regions and the brighter, denser, and higher temperature areas of the solar corona. This wavelength is commonly used to detect open magnetic field regions such as coronal holes and solar dimmings.

To identify and analyze CMEs we used observations from the Large Angle Spectroscopic Coronagraph (LASCO; Brueckner et al. 1995) system developed for the Solar and Heliospheric Observatory (SOHO) mission. Of the three coronagraphs, we used the externally occulted C2 instrument that observes the solar corona from 1.5–6  $R_{\odot}$ .

The flares in this study were identified by the NOAA Space Weather Prediction Center using the GOES X-ray Sensor (XRS; Hanser & Sellers 1996). XRS detects solar X-rays in two wavelength bands of approximately 0.5–3 Å and 1–8 Å. XRS uses a dual ion chamber design with beryllium windows and xenon or argon gas fills. The detected flares are archived by the NOAA National Center for Environmental Information.

In this study the dimmings were manually identified during the period 2010 December 1–2011 August 30 using STEREO-A, and 2010 December 1–2011 May 30 using STEREO-B. These periods were selected to ensure that the STEREO-A and -B satellites were close to right angles to SOHO (between 85° and 95°). This means that the CMEs were seen to propagate in the POS in SOHO observations. Figure 1 shows a cartoon of

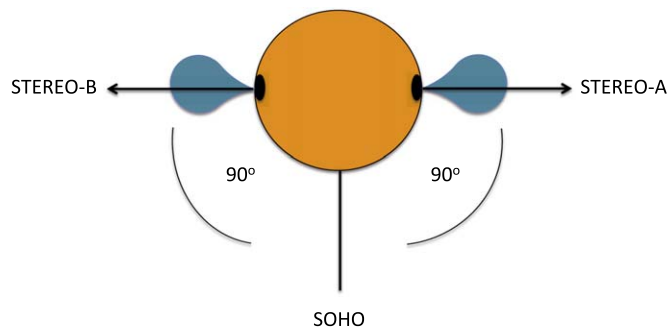


**Figure 1.** Cartoon showing the alignment of STEREO-A and -B, and the SOHO satellites seen from the direction of the solar north. The black regions shown on the solar disk represent dimmings (observed on-disk by STEREO-A and -B), and the plumes propagating away from the Sun represent the CMEs (observed off-disk by SOHO).

where SOHO and the STEREO twin satellites were located, seen from the solar north. It also shows the location of the observed dimmings (observed by STEREO-A and -B on the solar disk) and the propagation of the CMEs (observed by SOHO in the POS, off-disk).

An example of a dimming (named 20110509\_2130) and its associated CME is shown in Figure 2. On the left we can see the CME in a SOHO/LASCO/C2 white-light base-difference image. The magenta sector was manually selected and shows the region where the CME mass was calculated. In the top-right panel we see the STEREO-B/EUVI observation (converted from a full disk image into a Lambert equal-area projection map) with a teal rectangle highlighting the region of interest (ROI). The purple contour inside the ROI shows the detected

dimming. The bottom-right panel is the ROI sub-image showing a close-up of the dimming.

Using observations from the twin satellites we identified 53 dimmings in total. The dimmings showed high contrast against the surrounding quiet Sun and were clearly discernible in direct EUV images. We emphasize that no difference images were used in our dimming detection method, and the dimmings in our study are more accurately referred to as *footpoint dimmings* (Krista & Reinard 2017).

The identified dimmings were tracked throughout their lifetime using CoDiT (for more details see Krista & Reinard 2013 and Krista & Reinard 2017). The advantage of CoDiT is that it is able to identify the time and location of the dimming emergence and then track the dimming system as whole as it evolves: growing, fragmenting, merging, and shrinking. The algorithm tracks the dimming area and EUV intensity evolution, determines its lifetime, and the intensity drop in the dimming compared to the pre-eruption state. We refer to this intensity drop as the *change in the total EUV intensity*: this is calculated by subtracting the *post-eruption total EUV intensity* from the *pre-eruption total EUV intensity*. The post-eruption total EUV intensity is the sum of intensity within the dimming contour at the time of maximum area. The pre-eruption total EUV intensity is the total intensity of the dimming 3 hr before it first emerged (we use the maximum area contour but shift it to the correct location based on the time difference).

The CMEs were linked to dimmings based on the time and heliographic location of each dimming. The CDAW CME catalog ([https://cdaw.gsfc.nasa.gov/CME\\_list/](https://cdaw.gsfc.nasa.gov/CME_list/)) was used to first visually identify the correct CMEs. The CMEs in this catalog are detected using base-difference images created from

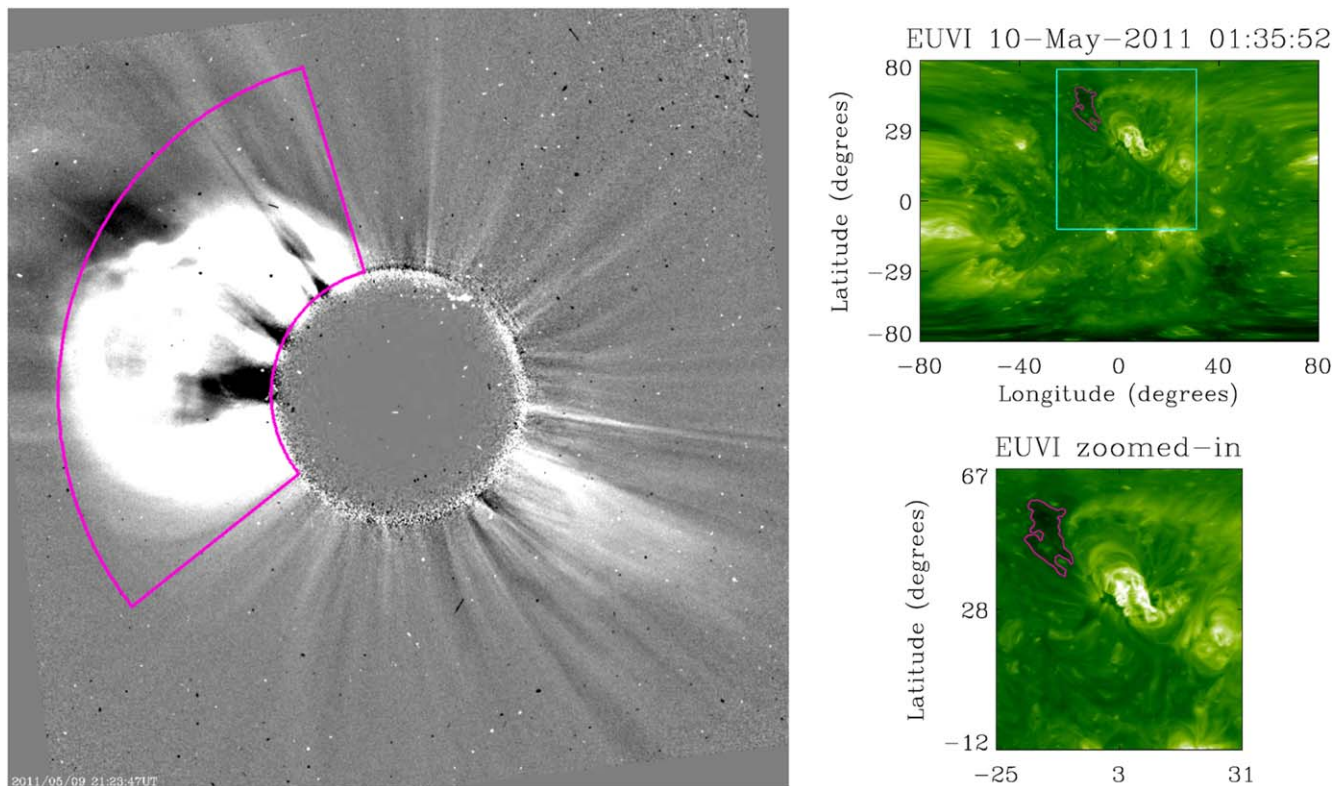


**Figure 2.** Left panel: CME observed with SOHO/LASCO on 2011 May 9. Top-right panel: the associated dimming identified in a STEREO-B/EUVI observation (seen here converted to a Lambert equal-area map). Bottom-right panel: a close-up of the dimming. The magenta sector in the left panel is used to calculate the CME mass, the teal box in the right panel shows the ROI, and the purple contour highlights the dimming boundary.

**Table 1**  
Dimming Properties ( $N = 53$ )

Property	Mean	Median	Stdev
Lifetime (hr)	11	6	15
$\Delta t_{\text{asc}}$ (hr)	2	1	3
$\Delta t_{\text{desc}}$ (hr)	9	4	13
Max area ( $10^3 \text{ Mm}^2$ )	4.8	4.5	4.3
Pre $I_{\text{EUV-TOT}}$ ( $10^4 \text{ DN}$ s)	6.2	5.1	5.4
Post $I_{\text{EUV-TOT}}$ ( $10^4 \text{ DN}$ s)	2.1	1.8	1.6
$\% \Delta I_{\text{EUV-TOT}}$	62	63	14

SOHO/LASCO/C2 coronagraph observations. We were able to pair 42 of our dimmings with CMEs.

Once the dimmings and CMEs were linked, we used C2 coronagraph observations and the CALC\_CME\_MASS and SCC\_CME\_MASSIMG2TOTAL procedures available in SolarSoft to manually select the CME sector and calculate the CME mass for each event. We selected the CME detection times to allow for the CMEs to appear at their largest extent without any parts being out of the field of view.

We were able to link 23 of the dimmings to flares. The flares associated with the dimmings were manually identified using the NOAA X-ray flare catalog (<https://www.ngdc.noaa.gov/stp/space-weather/solar-data/solar-features/solar-flares/x-rays/goes/xrs/>). This list used irradiances from GOES 1-15 XRS-B, which included a multiplicative scaling factor (for more information see <https://www.ngdc.noaa.gov/stp/satellite/goes-r.html>). The NOAA flare catalog provided the flare start times and the X-ray magnitudes for our present work and the values are consistent with those used in our 2017 work. In addition, we also used the JHelioviewer tool (Müller et al. 2017) to visualize the flare locations relative to the dimmings.

### 3. Results

Our study includes 53 dimmings identified and tracked in STEREO/EUVI A and B observations using the CoDiT algorithm. We were able to link 42 dimmings to CMEs and 23 dimmings to flares.

We determined the median and mean of the total dimming lifetime (6 and 11 hr), ascent time (1 and 2 hr), descent time (4 and 9 hr), and maximum area ( $4.5$  and  $4.8 \times 10^3 \text{ Mm}^2$ )—as shown in Table 1. These values are in good agreement with our past work (Krista & Reinard 2017). We also found that the typical drop in the dimming total EUV intensity from pre- to post-eruption is typically 63%.

The Pearson (P) and Spearman (S) correlation values for multiple dimming properties are listed in Table 2. We found strong relationships between the maximum area of the dimming and the post-eruption total EUV intensity ( $P = 0.86$ ,  $S = 0.76$ ), pre-eruption total EUV intensity ( $P = 0.63$ ,  $S = 0.91$ ), change

in total EUV intensity ( $P = 0.47$ ,  $S = 0.65$ ), and dimming lifetime ( $P = 0.54$ ,  $S = 0.75$ ). The post-eruption values are measured at the time when the dimming reached its maximum area. Pre-eruption values are measured 3 hr before the first emergence of the dimming (using the maximum area contour, shifted to the correct location). Note that the Pearson correlation demonstrates the degree of linear relationship between two properties, while the Spearman correlation can reveal a monotonic relationship that is not necessarily linear.

We found significant correlation between the dimming lifetime and the pre-eruption total EUV intensity ( $S = 0.57$ ), post-eruption total EUV intensity ( $S = 0.69$ ), ascent time ( $P = 0.84$ ,  $S = 0.71$ ), and descent time ( $P = 0.99$ ,  $S = 0.95$ ). There was also a strong linear correlation between the ascent and descent time ( $P = 0.76$ ). In Figure 3 we show a few of the scatter plots demonstrating significant relationships. The panels show the correlation between the dimming maximum area and the pre- and post-eruption total EUV intensity, the change in the total EUV intensity (top row, left to right, respectively), the total lifetime, and the ascent and descent time (bottom row, left to right, respectively). The left panel in Figure 4 demonstrates a strong linear correlation between the pre- and post-eruption total EUV intensity ( $P = 0.76$ ,  $S = 0.85$ ). The right panel shows that the total EUV intensity change has a very strong linear correlation with the pre-eruption total EUV intensity ( $P = 0.97$ ,  $S = 0.97$ ), and a moderate linear correlation with the post-eruption total EUV intensity ( $P = 0.59$ ,  $S = 0.73$ ). The  $p$ -values for all the above correlation coefficients were well below 0.01 in each case. Please note that  $p < 0.05$  is widely considered as statistically significant.

The CME mass showed a positive correlation with the change in total EUV intensity ( $P = 0.52$ ,  $S = 0.57$ ,  $p < 0.001$ ), dimming maximum area ( $P = 0.38$ ,  $S = 0.46$ ,  $p < 0.05$ ), pre-eruption total EUV intensity ( $P = 0.38$ ,  $p < 0.05$ ), and post-eruption total EUV intensity ( $P = 0.33$ ,  $S = 0.37$ ,  $p < 0.05$ ).

The flare duration showed a strong correlation with the dimming total EUV intensity change ( $P = 0.6$ ,  $S = 0.69$ ,  $p < 0.01$ ), a strong monotonic correlation with the dimming pre-eruption EUV intensity ( $S = 0.67$ ,  $p < 0.01$ ) and a moderate linear correlation with the dimming lifetime ( $P = 0.51$ ,  $p = 0.01$ )—these results are shown in Figure 5. We also found a strong positive monotonic correlation between the flare duration and the CME mass ( $S = 0.6$ ,  $p = 0.01$ ). We found no correlation between the flare magnitude and the dimming properties.

### 4. Discussion and Conclusions

#### 4.1. Observation and Terminology of Dimming Regions

We want to take the opportunity to emphasize the importance of understanding the difference between studying

**Table 2**  
Pearson (P) // Spearman (S) Correlation of Dimming Properties

	Pre $I_{\text{EUV-TOT}}$	Post $I_{\text{EUV-TOT}}$	$\Delta I_{\text{EUV-TOT}}$	Max Area ( $\text{Mm}^2$ )	$\Delta t_{\text{asc}}$ [hr]	$\Delta t_{\text{desc}}$ (hr)
Max area ( $\text{Mm}^2$ )	<b>0.63//0.91</b>	<b>0.86//0.76</b>	<b>0.47// 0.65</b>		<b>-//0.46</b>	<b>0.6// 0.77</b>
Lifetime (hr)	<b>-//0.57</b>	0.36// <b>0.69</b>	<b>-//-</b>	<b>0.54// 0.75</b>	<b>0.84//0.71</b>	<b>0.99//0.95</b>
	Pre $I_{\text{EUV-TOT}}$	Post $I_{\text{EUV-TOT}}$	$\Delta I_{\text{EUV-TOT}}$	Max area ( $\text{Mm}^2$ )	Lifetime (hr)	$m_{\text{CME}}$ (g)
$m_{\text{CME}}$ (g)	0.38//-	-//0.37	<b>0.52//0.57</b>	0.38// <b>0.46</b>	<b>-//-</b>	
Flare duration (hr)	<b>0.54//0.67</b>	<b>-//-</b>	<b>0.6//0.69</b>	<b>-//-</b>	<b>0.51//-</b>	<b>0.59//0.61</b>

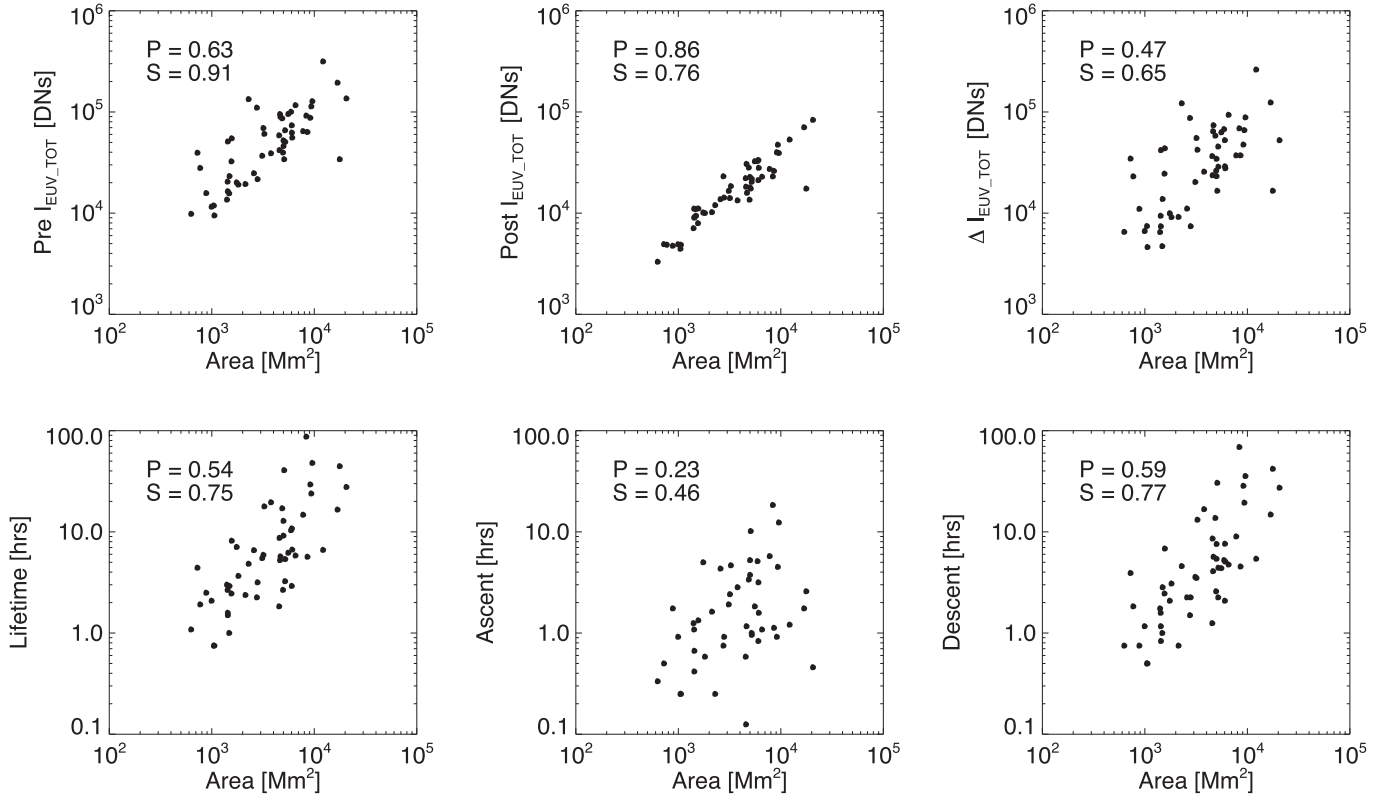


**Figure 3.** Scatter plots showing the correlation between the maximum dimming area and the dimming pre-eruption (top-left panel), post-eruption (top-middle panel), and change in total EUV intensity (top-right panel). The bottom panels show the correlation between the maximum dimming area and the dimming lifetime (left panel), ascent time (middle panel) and descent time (right panel).

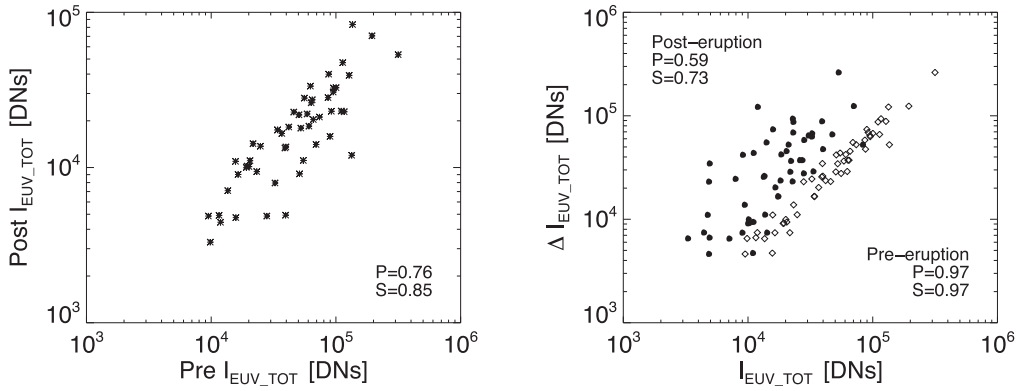


**Figure 4.** Left panel: scatter plot showing the correlation between the pre-eruption and post-eruption total EUV intensity. Right panel: a scatter plot showing the correlation between the change of total EUV intensity and the pre- and post-eruption total EUV intensity (shown in white diamonds and black disks, respectively).

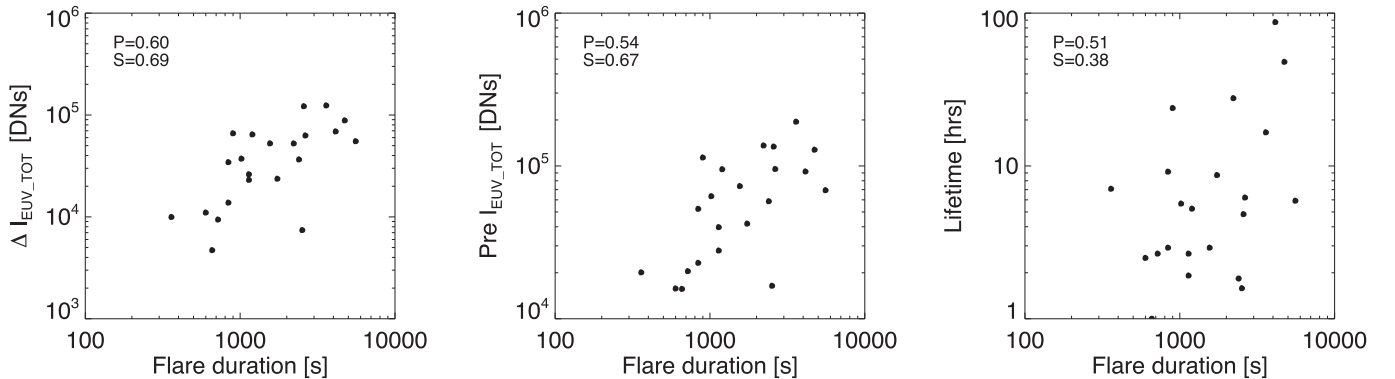


**Figure 5.** Scatter plots demonstrating the correlation between the duration of the X-ray flares and the total EUV intensity change (left panel), pre-eruption total EUV intensity (middle panel) and lifetime of dimmings (right panel).

dimming using direct EUV observations and difference images.

Direct EUV observations allow the imaging of footpoint dimmings: the primary mass evacuation sites at the footpoints of eruptive loop structures. Difference images, however, show the mass evacuation site combined with the rising CME plasma (footpoint and projection dimming). There is an important difference between these dimmings in terms of their physical structure and behavior. Footpoint dimmings are transient coronal holes that are created from a closed magnetic configuration that opens up due to an eruption, releasing high density plasma. Following magnetic reconnection, the CME plasmoid disconnects, and the open magnetic structure closes down and starts to refill with plasma. The low-corona part of this process can be studied through the evolution of the footpoint dimmings: the open region gradually grows, splits, merges, and eventually shrinks and disappears. We can directly observe the boundary of the footpoint dimmings, as they are distinct and sharp against the surrounding bright, high density regions. The boundaries of the projection dimmings are less distinct. This is due to the fact that the difference images show the transition of the plasma as it rises in altitude, evacuating the footpoint region and becoming the CME plasma plume that leaves the Sun. It is continuously expanding, its boundary gradually becoming more diffuse and fading into the background, as the CME propagates away from the Sun.

#### 4.2. Relationship between Dimmings, CMEs, and Flares

We performed our analysis for the unique quadrature period (2010 December–2011 August) when the STEREO-A and -B satellites were approximately at right angles with the SOHO satellite. In this period we identified 53 dimmings with the STEREO-A and -B EUVI instruments and were able to link 42 of the dimmings to CMEs detected with the SOHO/LASCO/C2 instrument. We were also able to link 23 dimmings to flares listed in the NOAA X-ray flare catalog.

The goal of this project was to investigate the relationship between dimming properties and their eruptive counterparts. In our previous work (Krista & Reinard 2017) it was unclear to what extent the correlation was influenced by inaccuracies in the mass measurements, as the analyzed CMEs propagated at a wide range of angles. It is known that the larger the CME propagation angle is relative to the POS, the larger the uncertainties are in the mass calculations (Vourlidis et al. 2010). Hence, in the work presented here, we re-analyze the relationship between dimmings and their associated CMEs in a unique scenario, when the CMEs are observed in the POS.

In our previous work, 42% of the dimmings were linked to CMEs (Krista & Reinard 2017) and we found a nonlinear, moderate correlation between the dimming EUV intensity properties and the CME mass, CME kinetic energy, and the flare duration. In our current work we were able to link 79% of the dimmings to CMEs, and we found a linear, moderate correlation between the CME mass and the change in the EUV intensity. We also found a monotonic, moderate correlation between the CME mass and the maximum dimming area—a relationship we did not observe in our previous study. These results show that the magnitude and linearity of the correlation between the dimming and CME properties depend on the observation angle of the CMEs. Our results further support the fact that the more the EUV intensity drops in a dimming region (indicative of the reduction of electron density), the more mass

is evacuated from the region. Furthermore, larger dimming areas can release more mass in the form of a CMEs. This result signifies the forecasting potential in observing the evolution of the total EUV intensity and the area of dimmings in order to estimate the associated CME masses.

In our 2017 work 27% of the dimmings were linked to flares and no correlation was found between the flare magnitude and the dimming properties. In our current work we were able to link 43% of the dimmings to flares. We did not find a correlation between the flare magnitude and the dimming properties. This result suggests that the energetics of the flare show no connection to the physical properties and evolution of the dimmings. However, we found the flare duration to have a strong, monotonic correlation with the dimming total EUV intensity change and dimming pre-eruption EUV intensity, and a moderate linear correlation with the dimming lifetime. We hypothesize that a longer flare duration is indicative of a longer reconnective process, which could facilitate a longer mass evacuation process. This is further supported by our result that shows a strong positive monotonic correlation between the flare duration and the CME mass, meaning that longer flare durations tend to be accompanied with larger mass evacuations through CMEs. It is important to note that flares appear to accompany dimmings less than half of the time and on the occasions they do, they typically occur at or before the dimming emergence. Therefore, dimmings provide little advantage in forecasting flare properties.




When studying the relationships between dimming properties, we found a strong relationship between the maximum area of the dimming and the pre- and post-eruption total EUV intensity, the change in the total EUV intensity and the dimming lifetime. From these relationships it is clear that larger dimmings are brighter, go through more intensity loss and they generally live longer. We also found the dimming maximum area to have a moderate to strong correlation with the ascent, descent, and total lifetime. This indicates that it takes longer to open up a larger closed region and consequently, a larger open region takes longer to close down again. We also found a monotonic, positive correlation between the dimming lifetime and the pre- and post-eruption EUV intensity, suggesting that long-lived dimmings are typically brighter both before and after the eruption. Furthermore, dimmings that are brighter before the eruption, tend to be brighter after the eruption. However, dimmings that are brighter before the eruption go through larger intensity drops.

In summary, the EUV intensity loss and the maximum area of a dimming could be useful in estimating the mass of the associated CME. This is particularly important in the case of Earth-directed CMEs when coronagraph observations are not available from multiple viewpoints. Furthermore, footpoint dimmings are of particular interest because these regions allow us to study the evolution of the flux rope configuration in the low corona. In our current and past publications we focused on the dimming properties and their relationship with their eruptive counterparts after the eruption has already occurred. In our future work we will focus more on understanding the changes that occur during and prior to the plasma evacuation phase.

This work was supported by the PROBA Guest Investigator program and by NASA grant No. NNX15AB91G issued through the NASA/LWS Program. This work was in part

supported by the National Science Foundation under Grant No. 1931062 issued through the NSF AGS/STR Program. The lead author would like to acknowledge the PROBA/SWAP science team at the Royal Observatory of Belgium. A.M. was supported through the NSF/REU program. SOHO is a project of international cooperation between ESA and NASA. EUVI observations are supplied courtesy of the STEREO Sun Earth Connection Coronal and Heliospheric Investigation (SECCHI) team.

#### ORCID iDs

Larisa D. Krista  <https://orcid.org/0000-0003-4627-8967>  
Drew Manning  <https://orcid.org/0000-0001-6778-0521>  
Matthew J. West  <https://orcid.org/0000-0002-0631-2393>

#### References

- Brueckner, G. E., Howard, R. A., Koomen, M. J., et al. 1995, *SoPh*, **162**, 357  
Dissauer, K., Veronig, A. M., Temmer, M., & Podladchikova, T. 2019, *ApJ*, **874**, 123  
Dissauer, K., Veronig, A. M., Temmer, M., Podladchikova, T., & Vanninathan, K. 2018a, *ApJ*, **855**, 137  
Dissauer, K., Veronig, A. M., Temmer, M., Podladchikova, T., & Vanninathan, K. 2018b, *ApJ*, **863**, 169  
Driesman, A., Hynes, S., & Cancro, G. 2008, *SSRv*, **136**, 17  
Hanser, F. A., & Sellers, F. B. 1996, *Proc. SPIE*, **2812**, 344  
Krista, L. D., & Reinard, A. 2013, *ApJ*, **762**, 91  
Krista, L. D., & Reinard, A. A. 2017, *ApJ*, **839**, 50  
López, F. M., Cremades, H., Balmaceda, L. A., Nuevo, F. A., & Vázquez, A. M. 2019, *A&A*, **627**, A8  
Müller, D., Nicula, B., Felix, S., et al. 2017, *A&A*, **606**, A10  
Vourlidas, A., Howard, R. A., Esfandiari, E., et al. 2010, *ApJ*, **722**, 1522  
Wuelser, J.-P., Lemen, J. R., Tarbell, T. D., et al. 2004, *Proc. SPIE*, **5171**, 111